Elsevier Editorial System(tm) for Powder Technology

Manuscript Draft

Manuscript Number:

Title: Comparison of Velocimetry Methods for Horizontal Air Jets in a Semicircular Fluidized Bed of Geldart Group D Particles

Article Type: Research Paper

Keywords: Fluidization; Validation; PTV; PIV; Optical Flow

Corresponding Author: Dr. William D. Fullmer,

Corresponding Author's Institution: National Energy Technology Laboratory

First Author: William D. Fullmer

Order of Authors: William D. Fullmer; Jonathan E Higham, PhD; Casey Q LaMarche, PhD; Allan Issangya, PhD; Ray Cocco, PhD; Christine M Hrenya, PhD

Abstract: Image-based velocimetry methods have become a widely used method to characterize solids velocity fields in particulate devices; two of the most commonly used methods being particle image velocimetry (PIV) and particle tracking velocimetry (PIV). Often, PIV and PTV are used at different scales or resolutions. Here, both velocimetry methods are applied to same high-speed video dataset. The quantity of interest is the measurement of jet penetration depths of four opposing, horizontal high-speed air jets into a semi-circular particulate bed maintained near minimum fluidization. In addition, a novel method, optical flow velocimetry (OFV), is applied for the first time to particulate flows and compared to the well-known PIV and PTV methods. Results show favorable agreement: within 20\% over 120 different measurements. Generally, the PTV measurements fall between PIV and OFV. The grid-resolution used to resolve the velocity field was also studied, finding the PTV and OFV methods relatively insensitive.

Suggested Reviewers: George Klinzing
Chemical and Petroleum Engineering, University of Pittsburgh
klinzing@pitt.edu
Dr. Klinzing is a renowned expert on Pneumatic Conveying of Solids, Solids Processing and Electrostatics.

Franco Berruti
Chemical and Biomedical Engineering, Western University
fberruti@uwo.ca
Dr. Berruti is an accomplished and internationally recognized researcher with expertise in chemical reactor technologies, thermal cracking, conversion of heavy oils and biomass residues and organic wastes into value-added fuels and chemicals.

Jingsi (James) Yang
Thermal Sciences, National Energy Technology Laboratory
Jingsi.Yang@netl.doe.gov

Dr. Yang has a wide range of experience in the application of image-based methods for measurement of particulate experiments.

Disclaimer: Dr. Yang and first author have same affiliation, but we are neither collaborators nor colleagues.

Oscar Link
Departamento de Ingeniería Civil, University of Concepción
olink@udec.cl
Prof. Link has a wide range of experience in particle transport in atypical conditions, e.g., sediment transport, and transport of scalar properties in rivers, sedimentation of reservoirs, river engineering: intakes, channeling, bridging of bridges.

Elisabeth Bowman
Department of Civil and Structural Engineering, University of Sheffield
e.bowman@sheffield.ac.uk
Her research is aimed at understanding particulate-scale mechanisms of geomaterials under deformation, including roles of particle size segregation, creep and fracture that produce important and sometimes puzzling geotechnical phenomena. Questions being addressed:

* What is the role of particle breakage in the runout of large rock avalanches?
* How does particle size segregation and pore pressure influence the velocity and run out of debris flows? How does this affect barrier design?
* How can seepage induced internal erosion of fine particles be characterized towards increased safety of hydraulic structures such as dams and levees?
* Why and how do granular soils “age” (increase in strength and stiffness with time)?

The investigative tools she uses in her research include physical modelling, transparent soil, high speed imaging, PIV and PTV techniques, centrifuge, flume and element testing and field mapping.

Thomas Hagemeier
Thermal Process Engineering, Otto-von-Guericke University Magdeburg
Thomas.Hagemeier@ovgu.de
Dr.-Ing. Hagemeier is the first and corresponding author of a similar study comparing PTV and PIV in the same experiment, though on different HSV data (Hagemeier, et al. Chem. Eng. Sci., 131: 63-75, 2015).

Cover Letter

Professor Liang-Shih Fan
Dept. of Chemical & Biomolecular Engineering
The Ohio State University
Columbus, OH 43210

May 20, 2019

Dear Prof. L-S. Fan,

On behalf of my co-authors, I would like to submit our manuscript titled "Comparison of Velocimetry Methods for Horizontal Air Jets in a Semicircular Fluidized Bed of Geldart Group D Particles," for consideration of publication in *Powder Technology*.

In the ms, new experimental data is taken of a semi-circular bed of Group D particles with opposing horizontal air jets, similar to a previous study which considered a larger, lighter material (Fullmer et al. *AIChEJ*, 64: 2351–2363, 2018). Like typical experiments which utilize velocimetry methods for measurement, we only considered one method (PTV) in the previous study. Here, in addition to the new material, three velocimetry methods (PTV, PIV and OFV) are applied and compared. Further making this work unique, all three methods have been applied to the same high-speed video data set. Finally, this appears to be the first time OFV has been applied to particulate flow. We expect this work to be relevant and of interest to experimentalists using velocimetry methods. Further, the new data may also be of interest to the computational community, specifically as CFD-DEM validation data. For this purpose, we have taken care to quantify or estimate and report measurement uncertainties.

This work is original, has not been published previously and is not under consideration elsewhere.

Thanks for your time and consideration,
Will

William D. Fullmer, PhD
Leidos Research Support Team
National Energy Technology Laboratory
Morgantown, WV 26507

***Highlights (for review)**

- PIV, PTV and OFV are used to measure jet penetration depths in fluidized bed
- PIV results are largely within ±10% of PTV results with a negative bias
- OFV results are largely within ±10% of PTV results with a positive bias
- PIV shows a grid resolution dependence; PTV/OFV do not

***Graphical Abstract (for review)**

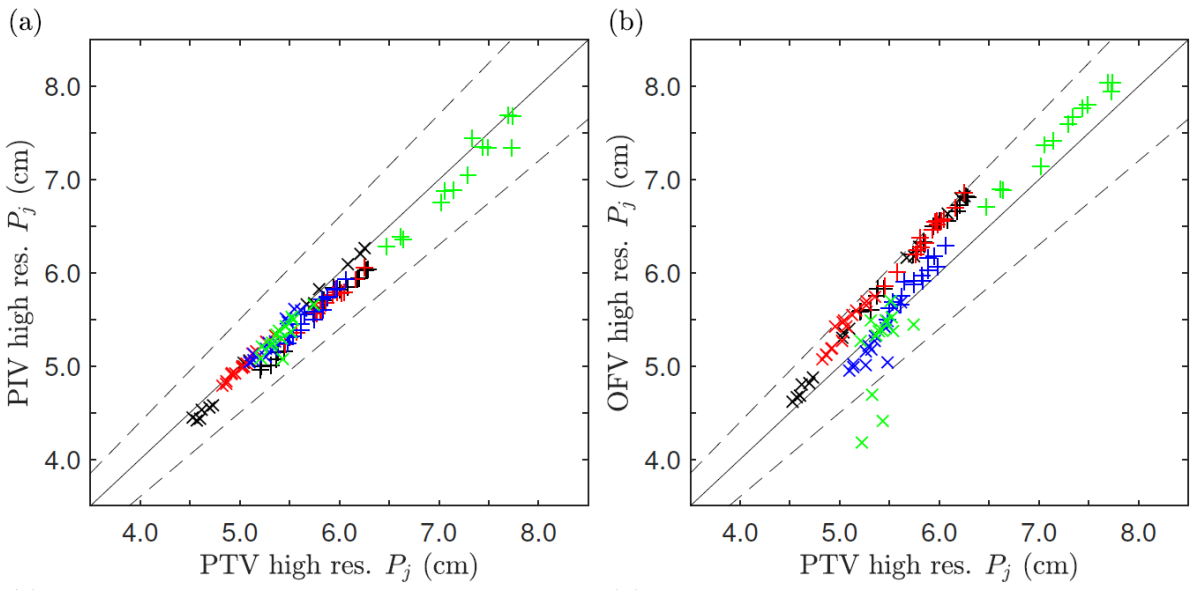

Parity plots comparing particle tracking velocimetry measurements against particle image velocimetry (a) and optical flow velocimetry (b) measurements on a high resolution grid of approximately one particle diameter in size.

***Abstract**

Image-based velocimetry methods have become a widely used method to characterize solids velocity fields in particulate devices; two of the most commonly used methods being particle image velocimetry (PIV) and particle tracking velocimetry (PIV). Often, PIV and PTV are used at different scales or resolutions. Here, both velocimetry methods are applied to same high-speed video dataset. The quantity of interest is the measurement of jet penetration depths of four opposing, horizontal high-speed air jets into a semi-circular particulate bed maintained near minimum fluidization. In addition, a novel method, optical flow velocimetry (OFV), is applied for the first time to particulate flows and compared to the well-known PIV and PTV methods. Results show favorable agreement: within 20\% over 120 different measurements. Generally, the PTV measurements fall between PIV and OFV. The grid-resolution used to resolve the velocity field was also studied, finding the PTV and OFV methods relatively insensitive.

Comparison of Velocimetry Methods for Horizontal Air Jets in a Semicircular Fluidized Bed of Geldart Group D Particles

William D. Fullmer[a], Jonny E. Higham[b], Casey Q. LaMarche[a,1], Allan Issangya[c], Ray Cocco[c], Christine M. Hrenya[a]

[a]*Department of Chemical and Biological Engineering, University of Colorado, Boulder, CO 80309 USA*
[b]*Department of Geography and Planning, School of Environmental Sciences, University of Liverpool, Liverpool L69 7ZQ, UK*
[c]*Particulate Solid Research, Inc., Chicago, IL 60632 USA*

Abstract

Image-based velocimetry methods have become a widely used method to characterize solids velocity fields in particulate devices; two of the most commonly used methods being particle image velocimetry (PIV) and particle tracking velocimetry (PTV). Often, PIV and PTV are used at different scales or resolutions. Here, both velocimetry methods are applied to same high-speed video data set. The quantity of interest is the measurement of jet penetration depths of four opposing, horizontal high-speed air jets into a semi-circular particulate bed maintained near minimum fluidization. In addition, a novel method, Optical Flow Velocimetry (OFV), is applied for the first time to particulate flows and compared to the well-known PIV and PTV methods. Results show favorable agreement: within 20% over 120 different measurements. Generally, the PTV measurements fall between PIV

Email address: hrenya@colorado.edu (Christine M. Hrenya)

and OFV. The grid-resolution used to resolve the velocity field was also studied with PTV and OFV methods proving relatively insensitive to the binning size. In addition to the comparison of velocimetry methods, this work extends the validation database of a related, previous study to a new 3mm ceramic material (Fullmer, LaMarche, Issangya, Liu, Cocco, and Hrenya 2018).
Keywords: Fluidization, Validation, PTV, PIV, Optical Flow

1. Introduction

High speed gas jets, typically vertically oriented, are commonly used to provide fluidization in engineering and industrial processes utilizing fluidized particulate beds [1, 2]. Though less pervasive, horizontal jets are also frequently found in industrial applications. Some examples include: providing additional flow to potentially stagnant or under-fluidized regions [3, 4], aiding solids mixing for material that may be difficult to fluidize such as biomass [5], introducing gas reactants [6], and controlling particle and agglomerate size distribution through attrition [7, 8, 9].

Horizontal air jets have also been studied numerically. However, past analyses have been limited to two-fluid model simulations [4, 10, 11] since typical experimental systems contained on the order of a billion particles or more. While particle counts on the order of 109 and beyond are still too computationally expensive for higher fidelity numerical methods such as coupled computational fluid dynamics-discrete element method (CFD-DEM), hardware and algorithmic improvements are continually expanding the range that CFD-DEM simulations are able to capture [12]. With this in mind, a set of experimental measurements have been conducted with the

purpose of generating validation data for CFD-DEM and related numerical methods that spans current capabilities to near future capabilities. The first set of measurements from this experimental campaign were recently provided by Fullmer et al. [13] for the largest diameter material, nominally 6 mm plastic beads. The most important quantity of interest measured in the experiments is the jet penetration depth, P_j, though mean and standard deviation of the bed pressure drop are also measured and reported. Most previous studies on horizontal jet used either visual observation [3, 14, 15] or void-based metrics [16, 4, 10, 11, 17, 18] to measure the jet penetration depth. Our previous work developed a novel momentum-based method to measure jet penetration depths using particle tracking velocimetry (PTV).

The next two materials studied in the experimental campaign are ceramic beads with (nominal) particle diameters of 3 mm, studied herein, and 1 mm, which will be considered in a futures study. The smaller, 1 mm ceramic material present a challenge to determining jet penetration depths with the momentum-based method, at least while relying on the PTV velocimetry method. Specifically, when the full bed width is imaged the particle are too small to be identified and tracked by traditional PTV. Conversely, if the camera is moved in to a location where the smaller particles can be identified, the jet penetration depth begins to extend beyond the field of view. Therefore, another image analysis method will be required for the smaller material.

The aim of this work is twofold: i) to extend the CFD-DEM validation database to a new material with a smaller particle size and hence a larger particle count and ii) to benchmark different velocimetry methods at this

intermediate particle size. The material considered here is nominally 3 mm ceramic beads and the static bed height is similar to that in the previous study, leading to nearly an order of magnitude increase in the particle count. In addition to PTV, two velocimetry methods which do not require identifying individual particles are applied: particle image velocimetry (PIV), which has been widely applied in the single-phase fluid flow community, and optical flow velocimetry (OFV), which is a relatively novel image analysis method as applied to fluid flow.

The remainder of this work is outlined as follows. In Section 2, the experimental setup is reviewed, and key dimensions are provided. The material characterization analysis is also outlined. The section ends by summarizing the flow conditions of the four sets of experiments analyzed in this work. The four image analysis methods are given in Section 3 with particular emphasis on how they differ from one another. Finally, in Section 4, the results of the different image analysis methods are provided and compared against one another at two different resolutions. Most of the presented results are quantitative assessments of the predicted jet penetration depths, however, representative qualitative comparisons are also provided in the Supplementary Material. The work is concluded in Section 5 with an outlook toward application to even smaller particles.

2. Experimental Setup and Conditions

2.1. Bed properties

In this section, the most salient features of the experimental device are provided; readers are referred to a previous work [13] for a full description.

The primary component of the test section is an acrylic fluidized bed. The geometry of the bed is sketched in Fig. 1 and the measurements, with associated uncertainties, are summarized in Table 1. The cross-section of the bed is approximately semi-circular (more accurately semi-elliptical) with a maximum (inside) depth of $D_{max} = 15.169$ cm and a width of $W = 28.58$ cm, at the front, flat face. However, we note that for the bed cross-sectional area, $A = W \times D_{max}/4 = 340.4$ cm^2, a conservatively large uncertainty of $\delta A = \pm 7.38$ cm^2 is applied in the conversion of the metered volumetric flow rate to superficial gas velocity in order to account for minor irregularities in the geometry. Compressed air is supplied to a plenum region below the bed. A drilled metal plate distributor (0.089-inch diameter holes in a 5/32-inch triangular pitch) covered with a fine wire mesh screen connects the plenum to the bed. The top (bed side) of the distributor plate is taken as zero height or elevation ($y = 0$).

Air jets are created by four steel tubes (quarter-inch OD) which penetrate the column horizontally, two on either side opposing one another at elevations of approximately 5 and 15 cm. The exact elevations and depths, z-distance away from the inside of the flat face of the bed, are provided in Table 1. The individual jets are identified by the notation lower left (LL), lower right (LR), upper left (UL), and upper right (UR). In this work, the ends of tubes are held flush with the inside walls of the bed and both upper (U) or both lower (L) jets are operated together.

2.2. Material characterization

The 3 mm ceramic beads used in this work were characterized using the same methods as the previous 6 mm plastic beads (Fullmer et al 2018). The

methods are briefly outlined below. The key data metrics are summarized in Table 2 and the raw data is provided as supplementary material.

Image analysis methods were used to measure the individual, particle-level properties. Particles were affixed to microscope slides for imaging and then processed to determine area and perimeter, which were then used to calculate particle diameter and sphericity [19, 20] based on the projected area [21]. The median particle diameter from 70 measurements was $d_{p50} =$ 3.068 mm, slightly lower than the mean diameter. The maximum spread of 70 diameter measurements normalized by the mean is 19.2%.

Particle coefficients of restitution and kinetic (sliding) friction are measured with the aid of a porcelain slab. Maximum particle rebound heights after bouncing off the slab were recorded and analyzed ImageJ to determine the restitution coefficients. To measure the coefficient of friction, four particles were glued to the corners of small, thin glass plates (microscope slides). The porcelain slab was then inserted into an inclined, humidity-controlled box [22]. The particle sleds are released from the top and slide down the length of the slab. The measurements are recorded by high-speed video illuminated by a black light. A dot of UV paint on the back of each sled is used to track the sled motion with an in-house Matlab code which estimates the sled acceleration, used to calculate the kinetic friction coefficient [23]

Water displacement was used to measure particle density. In order to displace a sufficient amount of water to make an accurate volume reading, density could only be measured as a bulk property. Therefore, the particle density, ρ_p reported in Table 2 only gives the minimum and maximum recorded densities.

Before the experiments are carried out, the bed was filled with material to a height roughly equal to the width of bed width. The bed was then operated in a well-fluidized state for several minutes to reach an equilibrium state. The bed height was then measured ten times, re-fluidizing and returning to a static condition after each measurement. The mean bed static bed height was determined to be 33.92 cm, roughly double the height of the upper jets.

Finally, the minimum fluidization velocity is measured by tracing out a fluidization curve. All air jets remain off and the distributor flow is incrementally increased by a volumetric flow rate of 5 standard cubic feet per minute SFPM (approximately 0.1363 m/s). The bed pressure drop, Δp_{bed} is measured by a set of Honeywell pressure transmitters (Model STD904-E1A-00000-AN.ZS.MB.1C+XXXX) connected with 1/4-inch polyethylene tubing to pressure taps mounted on the back of the bed equipped with high-porosity brass snubbers (McMaster-Carr size 40-45 micron, Part No. 4034K2, `www.mcmaster.com`). The lower pressure tap used for measuring Δp_{bed} is located at an elevation of $y = 70.36 \pm 1.588$ mm. The elevation of the second pressure tap is well above the bed, over a meter above the static bed height. At each flow condition Δp_{bed} is recorded for 1 minute at 100 Hz. Once fluidization is reached, four additional conditions are measured and averaged for the fully fluidized pressure drop. The condition near fluidization is neglected and the remaining unfuidized data are fit with a quadratic regression. The velocity corresponding to the intersection of the unfluidized pressure drop curve and the average fully-fluidized pressure drop is taken as the minimum fluidization (superficial) velocity, U_{mf}. The procedure was repeated three times to find $U_{mf} = 1.3557 \pm 0.0451$ m/s. The Wen-Yu correlation [24] pre-

dicts a minimum fluidization velocity 10% higher than the measured value, $U_{mf}^{\mathrm{WY}} \approx 1.5$ m/s.

2.3. Flow conditions

In this work, experimental data collected at four different operating conditions are considered. The superficial gas velocity of the distributor, U, is provided at either approximately 90% or 110% of U_{mf}. Additional fluidization is provided via either the lower (L) or upper (U) opposing high-speed air jets. The exit plane of the jets are placed as flush as possible with the inside wall of the bed with an estimated measurement uncertainty of approximately 3.18 mm; see Table 1 for locations of the jets. The measured distributor and jet velocities for the four conditions, denoted 90L, 90U, 110L and 110U, are provided in Table 3. The uncertainties of the measurements include uncertainties due to the measured volumetric flow rate, the flow cross-sectional area, the measured back pressure and the recorded ambient temperature, see Eq. (3) of [13] for more details.

Five replicate experimental measurements are taken at each condition. The primary measurement considered in this work is the high-speed video (HSV) imaging analyzed in Sec. 4. In addition to the HSV recordings, bed pressure drop measurements are also recorded. Pressure taps are located in the back of the bed at elevations of $y_1 = 70.36 \pm 1.588$ mm and $y_2 = 1667 \pm 6$ mm above the distributor plate. The bed pressure drop is taken as the difference of these two measurements: $\Delta p_{bed} = p_g(y_1) - p_g(y_2)$. The Δp_{bed} measurements are recorded for 30 s surrounding the HSV recording (in time) at an acquisition rate of 100 Hz. Each measurement is decomposed into five 6 s segments on which time-averaged statistics, mean and standard

deviation, are computed and reported in the Supplementary Material. The segment-averaged mean and confidence intervals (CI) defined CI yet? for each condition is reported in Table 3.

3. Velocimetry Methods

Over the past half decade there have a been a number of contributions suggesting and improving correlation- and algorithmic-based methods to determine displacements within images sequences. These methods typically fall into three categories: tracking individual object centroids between image pairs (Particle Tracking Velocimetry [25, 26, 27, 28, 29, 26, 13]); using gridded regions to determine displacements from correlations (Particle Image Velocimetry) [30, 31, 32, 33, 34], or, less commonly, using image gradients to track regions of displacement (Optical Flow Velocimetry) [35].

Each of these methods have their advantages and disadvantages. In a recent study by [36] the performance of PIV and PTV are compared, finding PTV to provide better insights into the dynamics of particulate flows. However, the PIV method is more robust in nature; low quality and/or low resolution input data can still be used to determine displacements with PIV. Hence, a larger field of view can be used with PIV than PTV for a fixed particle size. For example, Hagemeier et al. [37] used PIV for full-bed measurements where PTV could only be applied locally. An aim of the present study is to understand how these velocimetry methods compare against one another on the same HSV dataset.

Of the three methods, PTV has seems to have been used the most in fluidization and particle technology literature [38, 39, 40, 41, 42, 43, 44, 13].

However, PIV has also seen widespread use in the field [45, 46, 47, 48]. To the authors' knowledge, there have been no previous studies which have investigated the use of OFV in particulate flows. This study will aim to show its applicability.

3.1. Particle Tracking Velocimetry (PTV)

Currently many variants of PTV exist, all with the primary objective to determine the Lagrangian path of individual objects based on their centroids. In PTV this is typically done by first identifying objects for tracking through image analysis techniques such as binarization and thresholding. Then, the centroids of each object identified for tracking are calculated and matched with the centroids in adjacent frames that are believed to be the same object. In this work, we use an in-house, PTV code used in our previous study Fullmer et al. [13]. The PTV algorithm uses the watershed method [49] to isolate particles and requires that a particle be identified in at least three frames to be used for tracking. Due to the high frame rate and relatively small displacements of the particles in this study, a simple nearest neighbor approach is used; for interested readers we note that more sophisticated methods for particle identification, e.g., correlation methods [50], relaxation methods [51] and polynomial fitting [52, 53], also exist for PTV.

3.2. Particle Image Velocimetry (PIV)

Particle Image Velocimetry [54] is a Euclidean based method which determines displacements of regions of images (interrogation windows) based on correlations typically in the Fourier domain. The method compares the

interrogation windows from one image to the next image, determining displacements based on maximum correlations. The size of the interrogation windows is set by the user and it is common for them to overlap and often multiple size interrogation window are used. We stress that for PIV the interrogation window, or grid, is inherent in the velocimetry algorithm itself; it is not simply a post-processing step as in the case of PTV and OFV. To further increase the accuracy of the method, Gaussian distributions are fitted to correlation peaks allowing for 'sub-pixel' accuracy [55]. In this study, we use an in-house PIV code based on the PIVlab algorithm developed by Thielicke and Stamhuis [56], previously used by Higham et al. [57].
(Jonny, I would like to mention the 50% overlap somewhere in here and any other important algorithm setting.)

3.3. Optical Flow Velocimetry (OFV)

Optical Flow Velocimetry is a term coined in this study; the method we are presenting is the Lucas-Kanade estimation of the Optical Flow Equations [35, 58, 59]. The Optical Flow Equations are based on image intensity gradients of every pixel in an image. The Lucas-Kanade methods simplifies these equations by reducing the inputs via a least means square approach, under the assumption localized regions have constant motions. This method is commonly used in computer vision applications [60, 61, 62] but has more recently been successfully used in fluid mechanics applications [63, 64]. From this method it is possible to determine Lagrangian paths similar to PTV based on correlations as in PIV, but without the need to first determine centroids of objects within the images. In this work, we use the recently developed, open-source PTVResearch [65] code for OFV calculations.

3.4. Post-processing setup

As in our previous work [13] HSV imaging is taken to capture particle motion near the flat, front face of the bed. The camera (Vision Research Phantom v7.2) settings for these experiments are an acquisition rate of 1000 frames per second (fps), an exposure time of 151.75 μs, a resolution of 800×600 pixels (although this is cropped to the region of interest during post-processing) and a memory storage of 17696 frames. Each of the four experimental conditions is repeated five times and the HSV of each run is decomposed into three 5.8 s segments for a total of 30 video segments per condition.

In each case, post-processing of the HSV begins by (spatially) cropping the full frame to the region of interest. The left and right edges of the frame are brought in to the sides of the bed so that the width of the cropped frame is equal to the width of the bed. The lower edge of the frame is brought up to marker (the 77-inch mark on the adhered tape measure) which corresponds to a known elevation above the distributor plate The upper portion of the frame is left uncropped which extends, on average, 238.73 mm from 15.85 mmm to 254.58 mm above the distributor plate. This region is sufficiently large to capture the relevant bed hydrodynamics. In an effort to wash out uncertainty in locating the markers for the crop regions, the cropping procedure is repeated for each HSV. Consequently, the size of the resulting cropped frames vary slightly with an average resolution of 2.3871 pixels/mm. Hence, the diameter of the (nominally) 3 mm ceramic beads are resolved by 7 to 8 pixels, near the lower limit of the centroid-based PTV algorithm.

In order to compute continuous velocity fields, the velocimetry data is gridded and averaged over small spatial regions and the time interval (5.8 s segments). Since the grid size is part of the velocimetry method itself for PIV, we choose a grid size that is convenient for PIV and then apply that same grid for post-processing of PTV and OFV data which are averaged with a simple top-hat kernel. Two different grids are used in this study in order to investigate of the impact of the grid size: a "low resolution" $N_x \times N_y = 41 \times 34$ grid of approximately 7 mm per side and a "high resolution" $N_x \times N_y = 84 \times 70$ grid of approximately 3.4 mm per side.

4. Results

4.1. Mean jet penetration depths

Following the methodology set out in the previous study [13], the segment-(time) and bin-averaged solids velocity field, $V_s = (u_s(x_i, y_j), v_s(x_i, y_j))$ for $i \in [1, N_x]$ and $j \in [1, N_y]$, is non-dimensionalized into a scalar Froude number field, $Fr = |V_s| / \sqrt{g d_p}$, where $g = |\boldsymbol{g}|$ is the gravity magnitude. Finally, the jet penetration depths, P_j, or, specifically, $P_{j,\mathrm{L}}$ for the left and $P_{j,\mathrm{R}}$ for the right jet penetration depths, are measured as the furthest extent of the $Fr = 0.15$ iso-line from the adjacent wall in the "near-jet" region. The near-jet region is defined by simple geometric criteria: the half bed width from the adjacent wall to centerline and elevations from 0 to 70 mm above the jet penetration.

Example images of the resulting Fr contour plots are provided in Figs. S.1 to S.10 and all measured jet penetration depths are recorded in Tables S.X-XX in the Supplementary Material. Perhaps the first success of this work is

qualitative: the previous finding of $Fr \leq 0.15$ appears to be a good indicator of jet behavior in near U_{mf} slugging bed. Although the material has changed, both the current and previous [13] particles fell into Geldart Group D which produced large slugging bubbles in this bed; generalization of this criteria to bubbling regimes remains to be seen.

As in the previous study [13], the 90L condition is near an operational bifurcation point where jet-induced bubbling switches between the left and right sides. (Interest readers are referred to Sec. XX of the Supplementary Material and the previous study [13] for further details of this behavior.) For the three operating conditions which produce quasi-steady horizontal jets, i.e., the 90U, 110L and 110U cases, the average P_j results for the three velocimetry methods using the higher-resolution grid are compared in Table 4. Generally, we find that the jet penetration depth into the heavier ceramic beads are less than into a similar bed of lighter, albeit larger, plastic beads [13]. Again, we find that the 110U condition has the largest jet penetration depths. A slight side-to-side bias is observed which is believed to be due to geometrical irregularities. Reasonably good agreement between velocimetry methods–half the data in Table 4 are statistically similar–is found for the average. The influence of the grid resolution and the velocimetry method used to compute the velocity fields is explored further in Sections 4.2 and 4.3.

4.2. Resolution comparison

The first quantitative assessment we make is to investigate the impact of the grid resolution on the P_j predictions. Fig. 2 shows parity plots of P_j data computed on low resolution grids ($dx \approx 7$ mm) versus high resolution grids

($dx \approx 3.4$ mm). The first observation is that the grid does not significantly impact the results in any method as all data are quite close to the (zero-discrepancy) 1:1 line. Of the three, PIV shows the most scatter and OFV appears to have the tightest fit. Another positive result contained in Fig. 2 is that there does not appear to be considerable systematic biases from one operating condition to another. However, it does appear that the largest jet penetration depths occur on the right and the smallest jet penetration depths occur on the left.

To further highlight the impact of grid resolution, we consider the difference between the P_j predictions. It is tempting to take the difference between the low resolution result and the high resolution result as an error, however we do not have sufficient evidence to consider one more accurate (correct) than another. Hence, we define the discrepancy as

$$\delta_{yx} = \frac{y_i - x_i}{(y_i + x_i)/2}, \tag{1}$$

where x and y are P_j data and i is agglomerated over each segment, all experimental replicates, and both sides of the bed. The resolution discrepancy δ_{yx} of the parity plots of Fig. 2 are agglomerated into empirical cumulative distribution functions (ECDFs) using Eq. (1) with y as low-resolution measurements and x as high-resolution measurements. The three resulting resolution discrepancy ECDFs are provided in Fig. 3 which highlights some of the previous observations. Indeed, the OFV method shows the least grid sensitivity, generally between $\pm 1\%$. The PTV method also shows little grid sensitivity, largely between $\pm 2\%$. As expected, PIV shows the largest grid sensitivity of the three velocimetry methods, however, it is still a fairly good result with most discrepancy below 5% (in magnitude). The sign of the PIV

resolution discrepancy is perhaps more important than the magnitude. While the PTV and OFV resolution ECDFs are centered near zero; PIV shows a bias with the low resolution grid under-predicting the high-resolution grid. Again, the bias observation is somewhat expected. With PIV, the grid is inherent in the velocimetry algorithm itself. As the grid size increases, the area over which displacements are measured increases, leading to a more diffused measurement.

4.3. Velocimetry method comparison

Finally, we compare the different velocimetry methods in point-by-point basis similar to the previous resolution assessment. Figure 4 displays parity plots comparing all measurements from PIV and OFV against PTV. The method-to-method parity plots of Fig. 4 show a wider spread than the (single method) resolution comparison in the parity plots of Fig. 2. However, the overall scatter due to the different methods, while non-negligible, appears to be tolerable. Compared to PTV, most of the scatter from PIV and OFV measurements fall within $\pm$ 10%. There is a noticeable bias with PIV and OFV measurements falling on the low- and high-side, respectively, of the corresponding PTV measurements. It is somewhat comforting that the PTV method used in the previous study generally falls in the middle of the three measurements. Nonetheless, without a known solution, is it impossible to make an error assessment or determine which one of the three methods produces more accurate measurements.

The discrepancy between the methods can be highlighted by using Eq. (1) with y_i as PIV and OFV measurements and x_i as PTV measurements. The resulting method-to-method discrepancy is provided in Fig. 5. Again we see

mostly acceptable levels of discrepancy, $\pm$ 10%. In this presentation, the resolution dependence also becomes apparent. The OFV vs. PTV comparison give nearly identical discrepancy distributions, a reassuring result given that the gridding is only a post-processing step for both velocimetry methods. On the other hand, the PIV vs PTV comparison shows a moving bias, with the discrepancy distribution shifting closer to zero moving from low to high resolution grid. The shift can be explained by the spatial correlation algorithm of PIV: this low resolution grid is tracking mean displacements of spatial regions which contain information from several particles ($dx \times dy/d_p^2 \approx 5.0$) whereas the high resolution grid more closely approximates individual particle tracking ($dx \times dy/d_p^2 \approx 1.2$).

5. Summary and Outlook

The present work builds on a previous study of opposing, high-speed, horizontal air jets penetrating into a semi-circular particle bed uniformly fluidized slightly below and above minimum fluidization [13]. Here, the material has been changed from (nominally) 6 mm plastic beads to ceramic beads with approximately half the diameter (nominally 3 mm) and over twice the density ($\rho_p \approx 2615$ kg/m^3). The primary quantity of interest in this study is the jet penetration depth, P_j, which is measured by applying velocimetry methods to high-speed video data. Time-averaged mean and standard deviation of the bed pressure drop is also measured and reported.

Three velocimetry methods are used to measure (momentum-based) jet penetration depths: PTV, particle image velocimetry (PIV) and Optical Flow Velocimetry (OFV). On the whole, the three methods compare quite

favorably. The averaged jet penetration depths show several overlapping error bars indicating that the error incurred by a given velocimetry method may be on par with the inherent variability of the experiments (i.e., replicate-to-replicate differences). A detailed comparison of the results show that both new methods (i.e., not used in the previous study [13]) have discrepancies within $\pm$ 10% of the PTV method. However, a noticeable bias exists with OFV generally falling above PTV and PIV below PTV. Additionally, all results were computed with two different grid resolutions: a low resolution grid roughly twice the particle scale and a high resolution roughly equal in size to the particle scale. Both the PTV and OFV methods, for which the gridding is simply a post-processing step, show very little resolution dependence. The PIV method, for which the gridding is inherent in the algorithm, shows a noticeable, yet understandable, resolution dependence. As may be expected, the discrepancy between PIV and PTV was found to decrease with the grid size.

It is worth noting that the current work is the first time OFV has been applied to fluidization or granular flows. The results show that OFV may be a very promising technology for future studies in the field of particle technology. Future work will seek to further test the robustness of the OFV method on smaller 1 mm diameter particle material which is too fine for PTV to resolve (at full bed scale).

While all velocimetry methods compared favorably, one can not help but wonder which of the three methods is correct, or, at least, more accurate. Some codes, such as the National Energy Technology Laboratory's recently released, open source Tracker (`mfix.netl.doe.gov/tracker`) PTV code, are

distributed with validation cases. However, it is difficult to extrapolate the error from simple, idealized conditions to more realistic conditions, such as those examined in this work. Future effort on the verification of velocimetry codes specifically for the dense granular suspensions frequently encountered in fluidization and particle technology would be welcomed, perhaps rising to the level of the single-phase flow verification community represented by the PIV challenge (`www.pivchallenge.org`).

Acknowledgment

This work was supported by the U.S. Department of Energy under Grant No. DE-FE0026298. The authors are grateful for discussions and support received from Rasa Kales, Jeff Logsdon, S.B. Reddy Karri, Shyam Sundaram, Matt Hankosky, John Findlay and Aaron Holt. We are indebted to Tracy Foy, Anthony Granata, Ryan Ellis, Mike Arrington, Haley Manchester, and Lucas Karasek for performing technical work. This work utilized the Summit supercomputer, which is supported by the National Science Foundation, the University of Colorado Boulder, and Colorado State University. The Summit supercomputer is a joint effort of the University of Colorado Boulder and Colorado State University.

[1] D. o. Kunii, O. Levenspiel, Fluidization engineering, Butterworth-Heinemann series in chemical engineering, Butterworth-Heinemann, Boston, 2nd edition, 1991.

[2] L.-S. Fan, C. Zhu, Principles of gas-solid flows, Cambridge University Press, 2005.

[3] J. Merry, Penetration of a horizontal gas jet into a fluidised bed, Transactions of the Institution of Chemical Engineers and the Chemical Engineer 49 (1971) 189.

[4] R. Hong, H. Li, H. Li, Y. Wang, Studies on the inclined jet penetration length in a gassolid fluidized bed, Powder Technology 92 (1997) 205–212.

[5] M. Deza, T. J. Heindel, F. Battaglia, Effects of mixing using side port air injection on a biomass fluidized bed, Journal of Fluids Engineering 133 (2011) 111302.

[6] T. Knoebig, J. Werther, Horizontal reactant injection into large-scale fluidized bed reactors–modeling of secondary air injection into a circulating fluidized bed combustor, Chemical Engineering & Technology: Industrial Chemistry-Plant Equipment-Process Engineering-Biotechnology 22 (1999) 656–659.

[7] S. M. Tasirin, D. Geldart, Experimental investigation on fluidized bed jet grinding, Powder Technology 105 (1999) 337–341.

[8] J. McMillan, C. Briens, F. Berruti, E. Chan, High velocity attrition nozzles in fluidized beds, Powder technology 175 (2007) 133–141.

[9] F. Li, C. Briens, F. Berruti, J. McMillan, Particle attrition with supersonic nozzles in a fluidized bed at high temperature, Powder Technology 228 (2012) 385–394.

[10] T. Li, K. Pougatch, M. Salcudean, D. Grecov, Numerical simulation of horizontal jet penetration in a three-dimensional fluidized bed, Powder Technology 184 (2008) 89–99.

[11] T. Li, K. Pougatch, M. Salcudean, D. Grecov, Numerical simulation of single and multiple gas jets in bubbling fluidized beds, Chemical Engineering Science 64 (2009) 4884–4898.

[12] R. Cocco, W. D. Fullmer, P. Liu, C. M. Hrenya, CFD-DEM: Modeling the small to understand the large, Chemical Engineering Progress (2017) in press.

[13] W. D. Fullmer, C. Q. LaMarche, A. Issangya, P. Liu, R. Cocco, C. M. Hrenya, Experimental data for code validation: Horizontal air jets in a semicircular fluidized bed of geldart group d particles, AIChE Journal 64 (2018) 23512363.

[14] P. Roach, The penetration of jets into fluidized beds, Fluid dynamics research 11 (1993) 197.

[15] C. Chyang, C. Chang, J. Chang, Gas discharge modes at a single horizontal nozzle in a two-dimensional fluidized bed, Powder Technology 90 (1997) 71–77.

[16] L. Chen, H. Weinstein, Shape and extent of the void formed by a horizontal jet in a fluidized bed, AIChE journal 39 (1993) 1901–1909.

[17] Q. Guo, C. Si, J. Zhang, Flow characteristics in a jetting fluidized bed with acoustic assistance, Industrial & Engineering Chemistry Research 49 (2010) 7638–7645.

[18] F. Wang, Z. Yu, Q. Marashdeh, L.-S. Fan, Horizontal gas and gas/solid jet penetration in a gas–solid fluidized bed, Chemical Engineering Science 65 (2010) 3394–3408.

[19] H. Wadell, Sphericity and roundness of rock particles, The Journal of Geology 41 (1933) 310–331.

[20] D. Kunii, O. Levenspiel, Circulating fluidized-bed reactors, Chemical Engineering Science 52 (1997) 2471–2482.

[21] I. Cavarretta, C. OSullivan, M. Coop, Applying 2d shape analysis techniques to granular materials with 3d particle geometries, in: AIP Conference Proceedings, volume 1145, AIP, pp. 833–836.

[22] C. Q. LaMarche, A. W. Miller, P. Liu, C. M. Hrenya, Linking micro-scale predictions of capillary forces to macro-scale fluidization experiments in humid environments, AIChE Journal 62 (2016) 3585–3597.

[23] C. LaMarche, P. Liu, K. Kellogg, C. Hrenya, Fluidized-bed measurements of carefully-characterized, mildly-cohesive (group a) particles, Chemical Engineering Journal 310 (2017) 259–271.

[24] C. Y. Wen, Y. H. Yu, A generalised method for predicting minimum fluidization velocity, AIChE Journal 12 (1966) 610–612.

[25] A. Armanini, H. Capart, L. Fraccarollo, M. Larcher, Rheological stratification in experimental free-surface flows of granular–liquid mixtures, Journal of Fluid Mechanics 532 (2005) 269–319.

[26] S. Warr, G. T. Jacques, J. M. Huntley, Tracking the translational and rotational motion of granular particles: use of high-speed photography and image processing, Powder Technology 81 (1994) 41–56.

[27] E. Azanza, F. Chevoir, P. Moucheront, Experimental study of collisional granular flows down an inclined plane, Journal of Fluid Mechanics 400 (1999) 199–227.

[28] W. Bi, R. Delannay, P. Richard, A. Valance, Experimental study of two-dimensional, monodisperse, frictional-collisional granular flows down an inclined chute, Physics of Fluids 18 (2006) 123302.

[29] M. Larcher, L. Fraccarollo, A. Armanini, H. Capart, Set of measurement data from flume experiments on steady uniform debris flows, Journal of hydraulic research 45 (2007) 59–71.

[30] C. Ancey, N. Andreini, G. Epely-Chauvin, Granular suspension avalanches. i. macro-viscous behavior, Physics of Fluids 25 (2013) 033301.

[31] S. P. Pudasaini, K. Hutter, S.-S. Hsiau, S.-C. Tai, Y. Wang, R. Katzenbach, Rapid flow of dry granular materials down inclined chutes impinging on rigid walls, Physics of Fluids 19 (2007) 053302.

[32] S. K. Bryant, W. A. Take, E. T. Bowman, Observations of grain-scale interactions and simulation of dry granular flows in a large-scale flume, Canadian Geotechnical Journal 52 (2014) 638–655.

[33] D. M. Hanes, O. R. Walton, Simulations and physical measurements of glass spheres flowing down a bumpy incline, Powder technology 109 (2000) 133–144.

[34] P. Jop, Y. Forterre, O. Pouliquen, Crucial role of sidewalls in granular

surface flows: consequences for the rheology, Journal of Fluid Mechanics 541 (2005) 167–192.

[35] J. J. Gibson, The perception of the visual world., Houghton Mifflin, Boston, 1950.

[36] D. Gollin, W. Brevis, E. T. Bowman, P. Shepley, Performance of piv and ptv for granular flow measurements, Granular Matter 19 (2017) 42.

[37] T. Hagemeier, M. Börner, A. Bück, E. Tsotsas, A comparative study on optical techniques for the estimation of granular flow velocities, Chemical Engineering Science 131 (2015) 63–75.

[38] B. Gopalan, F. Shaffer, A new method for decomposition of high speed particle image velocimetry data, Powder technology 220 (2012) 164–171.

[39] B. Gopalan, F. Shaffer, Higher order statistical analysis of eulerian particle velocity data in cfb risers as measured with high speed particle imaging, Powder technology 242 (2013) 13–26.

[40] F. Shaffer, B. Gopalan, R. W. Breault, R. Cocco, S. R. Karri, R. Hays, T. Knowlton, High speed imaging of particle flow fields in cfb risers, Powder technology 242 (2013) 86–99.

[41] T. Hagemeier, C. Roloff, A. Bück, E. Tsotsas, Estimation of particle dynamics in 2-d fluidized beds using particle tracking velocimetry, Particuology 22 (2015) 39–51.

[42] K. Vollmari, R. Jasevičius, H. Kruggel-Emden, Experimental and numerical study of fluidization and pressure drop of spherical and non-

spherical particles in a model scale fluidized bed, Powder Technology 291 (2016) 506–521.

[43] B. Gopalan, M. Shahnam, R. Panday, J. Tucker, F. Shaffer, L. Shadle, J. Mei, W. Rogers, C. Guenther, M. Syamlal, Measurements of pressure drop and particle velocity in a pseudo 2-D rectangular bed with Geldart Group D particles, Powder Technology 291 (2016) 299–310.

[44] Z. Jiang, T. Hagemeier, A. Bück, E. Tsotsas, Color-ptv measurement and cfd-dem simulation of the dynamics of poly-disperse particle systems in a pseudo-2d fluidized bed, Chemical Engineering Science 179 (2018) 115–132.

[45] J. Link, C. Zeilstra, N. Deen, H. Kuipers, Validation of a discrete particle model in a 2d spout-fluid bed using non-intrusive optical measuring techniques, The Canadian Journal of Chemical Engineering 82 (2004) 30–36.

[46] J. A. Laverman, I. Roghair, M. v. S. Annaland, H. Kuipers, Investigation into the hydrodynamics of gas–solid fluidized beds using particle image velocimetry coupled with digital image analysis, The Canadian Journal of Chemical Engineering 86 (2008) 523–535.

[47] M. van Buijtenen, K. Buist, N. Deen, J. Kuipers, T. Leadbeater, D. Parker, Numerical and experimental study on spout elevation in spout-fluidized beds, AIChE Journal 58 (2012) 2524–2535.

[48] H. Zhang, M. Liu, T. Li, Z. Huang, X. Sun, H. Bo, Y. Dong, Experi-

mental investigation on gas-solid hydrodynamics of coarse particles in a two-dimensional spouted bed, Powder Technology 307 (2017) 175–183.

[49] F. Meyer, Topographic distance and watershed lines, Signal processing 38 (1994) 113–125.

[50] W. Brevis, Y. Niño, G. Jirka, Integrating cross-correlation and relaxation algorithms for particle tracking velocimetry, Experiments in Fluids 50 (2011) 135–147.

[51] K. Takehara, T. Etoh, A study on particle identification in ptv particle mask correlation method, Journal of Visualization 1 (1998) 313–323.

[52] C. Cierpka, B. Lütke, C. J. Kähler, Higher order multi-frame particle tracking velocimetry, Experiments in Fluids 54 (2013) 1533.

[53] J. Weber, R. Breault, M. Bobek, S. Rowan, J. Yang, Tracker, an open-source particle tracking velocimetry (ptv) application applied to multiphase flow reactors, in: ASME-JSME-KSME 2019 Joint Fluids Engineering Conference, AJKFLUIDS2019-5181.

[54] R. J. Adrian, J. Westerweel, Particle image velocimetry, 30, Cambridge University Press, 2011.

[55] D. P. Hart, Piv error correction, Experiments in fluids 29 (2000) 13–22.

[56] W. Thielicke, E. J. Stamhuis, Pivlab-towards user-friendly, affordable and accurate digital particle image velocimetry in matlab, Journal of Open Research Software 2 (2014).

[57] J. Higham, W. Brevis, C. J. Keylock, A. Safarzadeh, Using modal decompositions to explain the sudden expansion of the mixing layer in the wake of a groyne in a shallow flow, Advances in Water Resources 107 (2017) 451–459.

[58] B. D. Lucas, T. Kanade, An iterative image registration technique with an application to stereo vision, in: Proceedings of the 7th International Joint Conference on Artificial Intelligence (IJCAI), Vancouver, BC Canada, Aug. 24–28, 1981, pp. 121–130.

[59] B. D. Lucas, Generalized image matching by the method of differences, Ph.D. thesis, Carnegie Mellon University, 1985.

[60] J. F. Cohn, A. J. Zlochower, J. J. Lien, T. Kanade, Feature-point tracking by optical flow discriminates subtle differences in facial expression, in: fg, IEEE, p. 396.

[61] J. J.-J. Lien, T. Kanade, J. F. Cohn, C.-C. Li, Detection, tracking, and classification of action units in facial expression, Robotics and Autonomous Systems 31 (2000) 131–146.

[62] S. Ali, M. Shah, A lagrangian particle dynamics approach for crowd flow segmentation and stability analysis, in: Computer Vision and Pattern Recognition, 2007. CVPR'07. IEEE Conference on, IEEE, pp. 1–6.

[63] G. M. Quénot, J. Pakleza, T. A. Kowalewski, Particle image velocimetry with optical flow, Experiments in fluids 25 (1998) 177–189.

[64] R. Yegavian, B. Leclaire, F. Champagnat, C. Illoul, G. Losfeld, Lucas–kanade fluid trajectories for time-resolved piv, Measurement science and Technology 27 (2016) 084004.

[65] J. Higham, PTVResearch, 2018.

Table 1: Dimensions of the semi-circular fluidized bed and locations of the horizontal air jet penetrations.

Bed property	Units	Measurement	Uncertainty ($\pm$)
Width, W	(mm)	285.8	1.588
Maximum depth, D_{mx}	(mm)	151.69	~ 3.18
Jet diameter, D_j	(mm)	3.86	< 0.01
LL jet elevation, y_{LL}	(mm)	51.46	1.588
LR jet elevation, y_{LR}	(mm)	54.56	1.588
UL jet elevation, y_{UL}	(mm)	154.33	1.588
UR jet elevation, y_{UR}	(mm)	153.06	1.588
LL jet depth, z_{LL}	(mm)	16.67	1.588
LR jet depth, z_{LR}	(mm)	17.46	1.588
UL jet depth, z_{UL}	(mm)	19.05	1.588
UR jet depth, z_{UR}	(mm)	17.46	1.588

Table 2: Summary of particle characterization data. Raw measurements of each property are reported in the Supplementary Material.

Particle property	Units	Measurement	95% CI (±)
Particle diameter, d_p	(mm)	3.113	0.043
Sphericity, ψ	–	0.943	0.001
Restitution coeff., e_{pp}	–	0.916	0.006
Kinetic friction coeff., μ_{pp}	–	0.217	0.004
Density, ρ_p	(kg/m^3)	2611 - 2619	
Static bed height, H_{bed}	(mm)	339.2	0.8
Minimum fluidization velocity, U_{mf}	(m/s)	1.3557	0.0451

Table 3: Summary of bed operating conditions during the four experiments. See Supplementary Material for additional Δp_{bed} data.

	U (m/s)	$U_{j,\mathrm{L}}$ (m/s)	$U_{j,\mathrm{R}}$ (m/s)	mean Δp_{bed} (Pa)	std Δp_{bed} (Pa)
90L	1.2318 ± 0.0962	199.5 ± 11.9	199.5 ± 11.9	3534.8 ± 8.3	27.5 ± 3.4
90U	1.2318 ± 0.0962	199.5 ± 8.0	199.5 ± 8.0	3363.0 ± 13.0	19.1 ± 0.9
110L	1.5025 ± 0.1005	199.1 ± 11.9	199.1 ± 11.9	3686.3 ± 8.3	49.2 ± 2.9
110U	1.5040 ± 0.1006	199.3 ± 8.0	199.3 ± 8.0	3642.2 ± 6.0	40.1 ± 2.1

Table 4: Averaged left- and right-side jet penetration depths computed on the high-resolution grid for all three velocimetry methods.

	90U		110L		110U	
	$P_{j,\mathrm{L}}$	$P_{j,\mathrm{R}}$	$P_{j,\mathrm{L}}$	$P_{j,\mathrm{R}}$	$P_{j,\mathrm{L}}$	$P_{j,\mathrm{R}}$
PIV	50.2 ± 0.6	56.9 ± 0.8	52.9 ± 0.7	55.8 ± 0.8	54.2 ± 0.6	72.1 ± 1.7
PTV	50.5 ± 0.6	58.9 ± 0.8	53.5 ± 0.6	57.5 ± 0.7	53.3 ± 0.7	70.3 ± 1.9
OFV	54.0 ± 0.8	64.0 ± 1.0	52.5 ± 0.9	59.0 ± 0.8	52.0 ± 1.8	74.8 ± 1.8

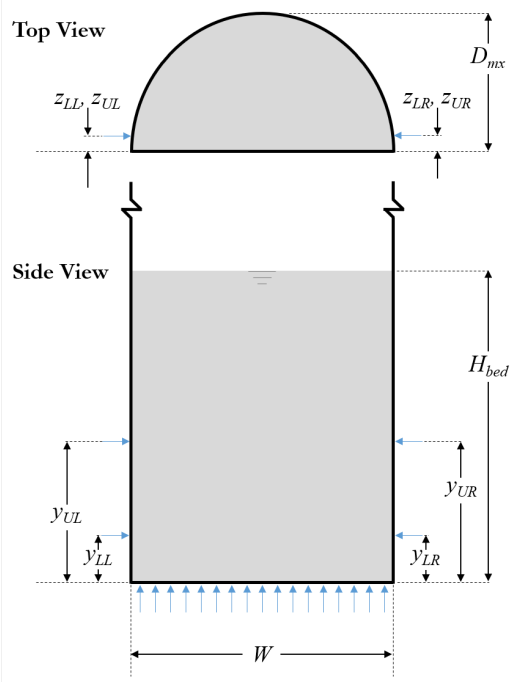

Figure 1: (Color online.) Sketch of the test section showing key features with dimensions provided in Table 1 (sketch not to scale).

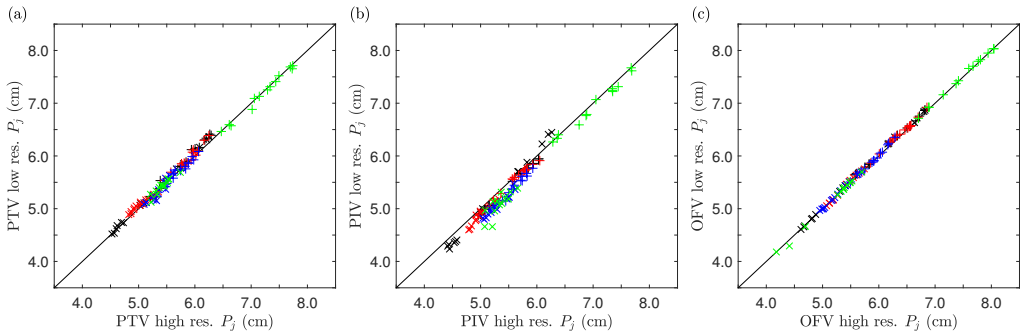

Figure 2: (Color online.) Parity plots comparing low-resolution to high-resolution grids for (a) PTV, (b) PIV, and (c) OFV. Key: (×) $P_{j,\mathrm{L}}$, (+) $P_{j,\mathrm{R}}$, black 90L, red 90U, blue 110L, green 110U. Solid line shows 1:1.

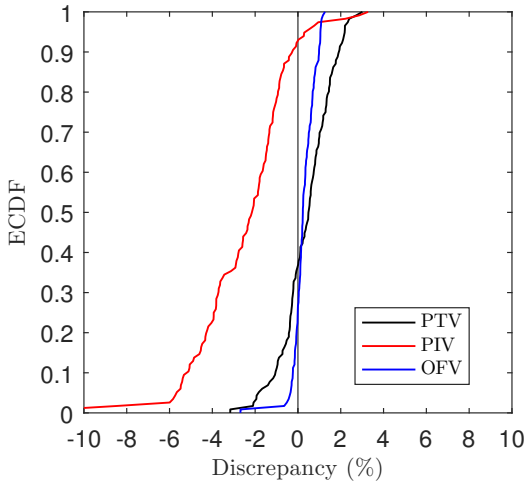

Figure 3: (Color online.) Cumulative distribution of the resolution discrepancy δ_{yx} between y = low-resolution and x = high-resolution.

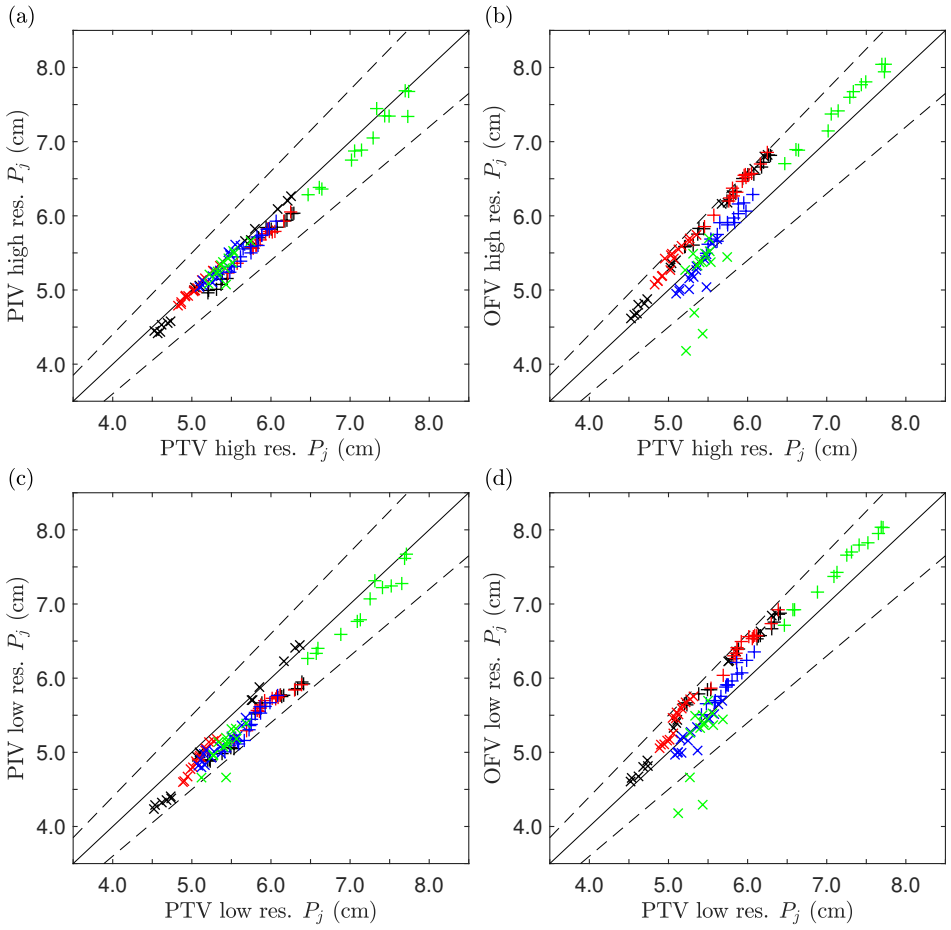

Figure 4: (Color online.) Parity plots comparing (a,c) PIV and (b,d) OFV velocimetry methods to the PTV velocimetry method at high (a,b) and low (c,d) resolutions. Key: (×) $P_{j,\mathrm{L}}$, (+) $P_{j,\mathrm{R}}$, black 90L, red 90U, blue 110L, green 110U. Solid line shows 1:1, dashed lines show ± 10%.

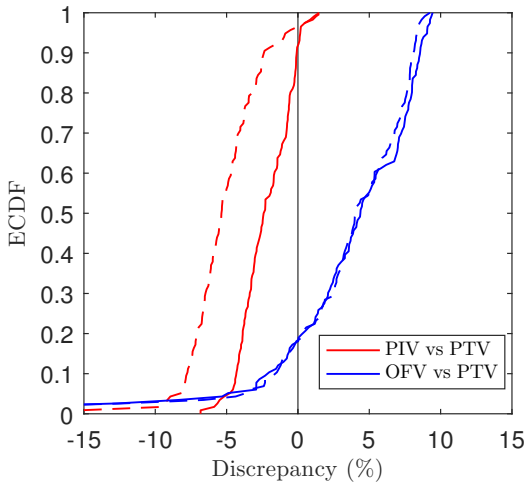

Figure 5: (Color online.) Cumulative distribution of the discrepancy δ_{yx} between velocimetry methods, y = PIV and OFV, x = PTV. Dashed and solid lines show measurements from low and high resolution grids, respectively.

Supplementary Material

Click here to download Supplementary Material: Supplementary_Material_R0.pdf